Chirped-Pulse Millimeter-Wave Spectroscopy of Rydberg-Rydberg Transitions

Kirill Prozument, Anthony P. Colombo, Yan Zhou, G. Barratt Park, Vladimir S. Petrović, Stephen L. Coy, and Robert W. Field

Phys. Rev. Lett. **107**, 143001 — Published 26 September 2011

DOI: 10.1103/PhysRevLett.107.143001

Chirped-Pulse Millimeter-Wave Spectroscopy of Rydberg–Rydberg Transitions

Kirill Prozument, Anthony P. Colombo, Yan Zhou, G. Barratt Park,
Vladimir S. Petrović,* Stephen L. Coy, and Robert W. Field†
Department of Chemistry, Massachusetts Institute of Technology, Cambridge, MA 02139

Transitions between Rydberg states of Ca atoms, in a pulsed, supersonic atomic beam, are directly detected by Chirped-Pulse Millimeter-Wave (CPmmW) spectroscopy. Broadband, high-resolution spectra with accurate relative intensities are recorded instantly. Free induction decay (FID) of atoms, polarized by the CP, at their Rydberg–Rydberg transition frequencies, is heterodyne-detected, averaged in the time domain, and Fourier-transformed into the frequency domain. Millimeter wave transient nutations are observed, and the possibility of FID evolving to superradiance is discussed.

PACS numbers: 32.80.Ee, 32.30.Bv, 32.80.Qk, 33.70.Fd

Atoms and molecules in highly excited Rydberg states [1] are a mostly unexploited state of matter. Millimeter-wave (mm-wave) spectroscopy is a high-resolution tool capable of characterizing the weak, anisotropic interactions between the Rydberg electron and the ion-core in atoms and molecules [2, 3]. In molecules, the exchange of energy and angular momentum between the Rydberg electron and the *not-round* molecular ion-core are, in extremely attenuated form, the most basic physical processes underlying chemical reactions. Strong long-range interactions between Rydberg species facilitate such cooperative effects as superradiance [4–11], cold plasma formation [12], and dipole blockade [13], which has been proposed for quantum gate implementation. Normally, in pulsed jet or magneto-optical trap/pulsed laser Rydberg experiments, transitions are signaled by detection of ions or electrons produced by pulsed field ionization or other schemes, as the mm-wave frequency is scanned one resolution element at a time. It takes $\sim 10^5$ molecular beam/laser/mm-wave pulses (15 hours at 20 Hz, 10 shots per 100 kHz resolution element) to scan 10 GHz.

Chirped Pulse Fourier-Transform Microwave spectroscopy, pioneered recently by Brooks Pate and coworkers [14, 15], has revolutionized the well-established field of rotational microwave spectroscopy. Chirped-Pulse Millimeter-Wave (CPmmW) spectroscopy is the extension of the technique to the mm-wave region [16].

Here we report a proof-of-principle observation of the CPmmW spectrum of electronic transitions between Rydberg levels of Ca atoms. The experimental setup is shown in Fig. 1. The vertically polarized pulsed (6 ns) tunable lasers, operating at 272 nm and 800 nm excite Ca atoms to their $4s36s\ ^1S_0$ Rydberg state via the intermediate $4s5p\ ^1P_1$ state (see insert in Fig. 2). A mm-wave pulse, the frequency of which is swept linearly in time, is generated by a frequency-up-converted arbitrary waveform generator (AWG) (4.2 Gs/s, Tektronix AWG710B). This chirped pulse polarizes all Rydberg–Rydberg transitions (creates coherences) for which the resonance frequency occurs within the frequency range of the chirp. These independent coherences undergo free induction decay (FID), the oscillating electric field of which is heterodyne-detected by mixing with a local oscillator. The down-converted FID signals, which result from successive chirps, are averaged in the time domain in a fast (12.5 GHz, 50 Gs/s, Tektronix DPO71254B) oscilloscope, until the desired signal-to-noise ratio (S/N) is achieved, and Fourier transformed into the frequency domain.

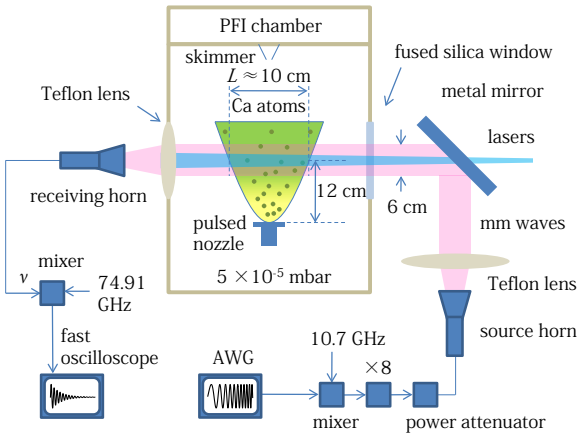

FIG. 1. Rydberg CPmmW experimental setup. Ca atoms are produced by laser ablation and supersonically co-expanded with He gas into vacuum [17]. The diverging laser beams, delivered through a 12 mm aperture in the metal mirror, excite Ca atoms to a selected Rydberg state. The chirped mm-wave pulses are broadcast from the source horn and the FID is collected by the receiving horn. The pulsed lasers and gas nozzle operate at a 20 Hz repetition rate, and are syncronized with the mm-wave pulses.

All resolution elements in a 0.5 GHz spectral range are sampled simultaneously in one pulse. This broadband spectral data acqusition allows recording of the entire spectrum with high resolution ($\sim$0.5 MHz) in a few seconds rather than a few hours and ensures accurate relative intensities of all spectral elements. The spectral range can be extended up to the full bandwidth of the spectrometer of 12.5 GHz [16]. The sensitivity of relative transition intensity data to interference effects in the matrix fit model supplements accurate transition frequencies

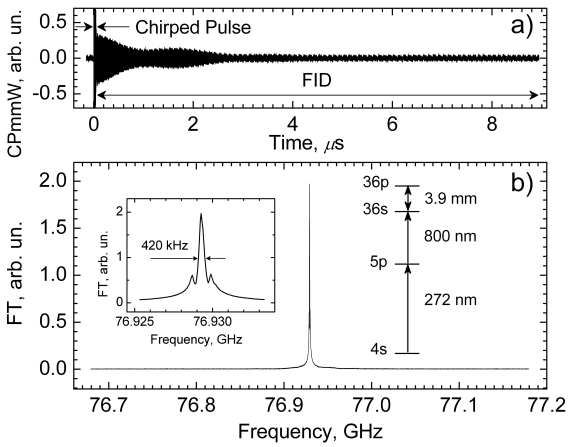

FIG. 2. CPmmW spectrum of Ca atoms. a) The 10 ns duration, 3.9 V/m ($\approx 1.4\times10^{-5}$ W), 0.5 GHz bandwidth chirped pulse centered around the $\nu = 76.9293$ GHz [21] $36p$–$36s$ transition, is followed by FID. Fine modulation is due to the 10 MHz Frequency Standard [16]. b) The spectrum is a (rectangular window) magnitude Fourier transform of the FID. The inserts show an up-close view of the line, which is split into the three Zeeman components with $\Delta\nu_{\rm FWHM} = 420$ kHz of the central peak, and the level diagram of Ca atoms.

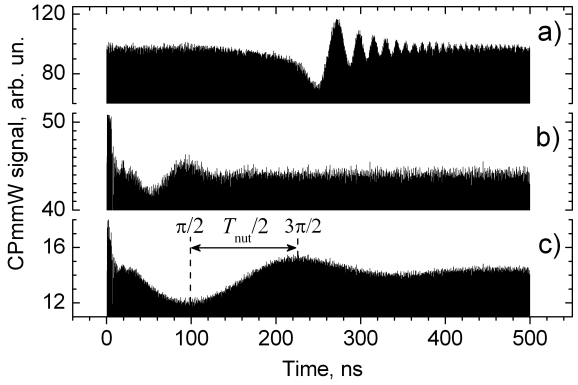

FIG. 3. Millimeter wave transient nutations (only the top portion is shown). a) The FID is initiated when the frequency of the chirped excitation pulse (500 ns duration) tunes through the Rydberg–Rydberg resonance. The frequency of the chirp is swept linearly in time away from resonance while that of the FID is constant; hence the frequency of the beat increases. b, c) Single frequency excitation pulse. b) $\mathcal{E}_0$=0.69 V/m is determined by measuring $T_{\rm nut} = 84$ ns; c) $\mathcal{E}_0$=0.23 V/m, $T_{\rm nut} = 250$ ns. When deducing $\mathcal{E}_{\rm FID}$ we took into account that approximately 60% of the detected signal comes from the mm waves that pass outside of the interaction volume.

(∼10 kHz precision), thereby enhancing the uniqueness and convergence of (both effective Hamiltonian [18] and Multichannel Quantum Defect Theory [19]) fit models.

The present CPmmW setup incorporates several essential features. The expanded laser and mm-wave beams intercept an *unskimmed* Ca atom beam providing about 70 cm^3 of interaction volume (length $L \approx 10$ cm, area ≈ 7 cm^2) with Rydberg atoms at a number density of $n \sim 10^6$ cm^{-3}. Maximizing the interaction volume allows an increase in S/N while keeping the number density of Rydberg species sufficiently low to avoid dipole–dipole dephasing. Downstream from the interaction region, the central part of the supersonic beam is selected by a 1 mm skimmer and enters the next chamber, which facilitates tuning the (steered) dye lasers to excite a specific Rydberg state with detection by pulsed field ionization (PFI) [17]. Locating the FID and PFI regions in separate chambers minimizes stray electric fields that are known [2, 20] to shift and broaden the mm-wave spectra of Rydberg–Rydberg transitions.

The chirped pulse followed by the FID signal and the corresponding CPmmW spectrum of the $36p$–$36s$ Rydberg–Rydberg transition in Ca atoms are shown in Fig. 2. 5000 averages of the FID in the time domain (about 5 min of acquisition time) are required to obtain S/N = 1000. The main contribution to the 420 kHz linewidth (characteristic time $T \approx 1$ μs) is from Doppler dephasing. The other contributions can be from (superradiant) population decay, the transit time of Ca atoms and dipole–dipole dephasing. Splitting of the line into three Zeeman components is due to the magnetic field of the Earth and the stray magnetization of the vacuum chamber, which have been partially compensated for by Helmholtz coils. The frequency separation of the satellite lines depends on the current in the Helmholtz coils. The laser energy was 0.5 mJ/pulse in each beam, and $n \lesssim 10^6$ cm^{-3}. Variation in number density n and in lineshape is expected due to instability in the ablation source.

Due to the kiloDebye transition dipole moments of Rydberg–Rydberg transitions [1, 8], a Rydberg CPmmW experiment operates in a qualitatively different regime from a rotational CP experiment [14, 16] where a typical transition dipole moment is ∼1 Debye. A low power CP can completely polarize the transitions and create an FID that is of comparable strength to the CP. Interference between the FID and the CP (transient nutation [11, 22–24]) is demonstrated in Fig. 3a. The interference beats can report important information about the system, such as number density, transition dipole moment or excitation field strength, and the dephasing rates of the driven two-level systems, thus complementing the spectral information obtainable from FID.

To analyze this interference, consider a single frequency resonant excitation pulse $E(t) = \mathcal{E}_0 \cos(2\pi\nu t)$ of constant electric field amplitude $\mathcal{E}_0$ (Figs. 3b, c, 4). While the excitation pulse is on, the CPmmW spectrometer detects both the excitation field $\mathcal{E}_0$ and the reemitted FID field $\mathcal{E}_{\rm FID}$, which interfere to give the observed pattern of mm-wave nutations. Increased laser energy (1 mJ/pulse in each beam) and, therefore, n, and no stray magnetic

field compensation were used in these measurements.

When $\mathcal{E}_0 \gg \mathcal{E}_{\rm FID}$ (Fig. 3b), the macroscopic polarization of the sample $\mathcal{P}$ and the $\mathcal{E}_{\rm FID}$ oscillate at the Rabi frequency, $\Omega_{\rm R} = \frac{\mu\mathcal{E}_0}{\hbar}$. The Ca atom $36p$–$36s$ electric transition dipole moment, μ, can be precisely calculated by the method of Ref. [25] to be 3439 D. Therefore, $\mathcal{E}_0$ can be determined from the nutation period $T_{\rm nut} = 2\pi/\Omega_{\rm R} = 2\pi\hbar/\mu\mathcal{E}_0$.

The decay time of the transient nutations in Figs. 3b, c is equal to about one nutation period and is, therefore, inversely proportional to $\mathcal{E}_0$. This suggests that the nutation dephasing mechanism is likely to originate from field-induced splitting (Mollow triplet) [26] of the Rydberg–Rydberg transition, perhaps, in combination with the field inhomogeneity of the mm wave beam. The field dependent dephasing would explain our observation that the strongest FID signal (Fig. 4) is detected after a $\sim \frac{\pi}{2}$ pulse, but not after $\sim \frac{3\pi}{2}$ or $\sim \frac{5\pi}{2}$ pulses of the same duration. Note that the linewidths in the spectra are not affected by this broadening as the spectra are transforms of FID, which is recorded in the absence of strong driving field. However, if the FID is sufficiently strong, it can be considered a driving field itself and can cause splitting and/or broadening of the lines. We show below that the condition for observing these effects, $\Omega'_{\rm R} = \frac{\mu\mathcal{E}_{\rm FID}}{\hbar} \gg 1/T$, is equivalent to the condition for superradiance.

The number density of Rydberg species can be estimated from the depth of the mm wave nutations. $\mathcal{P} = \mu n$ when the excitation pulse area reaches $\frac{\pi}{2}$ at the first *minimum* of the interference pattern. Having determined $\mathcal{E}_0$, $\mathcal{E}_{\rm FID}$ was evaluated at that point, using the trace in Fig. 3b, to be 3.3×10^{-6} esu = 0.099 V/m. Given that $\mathcal{E}_{\rm FID} = 4\pi^2\mathcal{P}\frac{L}{\lambda}$ [11, 24], where $\lambda = 3.9$ mm is the mm wave wavelength and $L \approx 10$ cm is the extent of the sample in the mm wave propagation direction (Fig. 1), we obtain $n \approx 1\times10^6$ cm^{-3} total $36s$ and $36p$ population.

When $\mathcal{E}_0 \sim \mathcal{E}_{\rm FID}$ (Fig. 4), the effective driving field $\mathcal{E}_{\rm eff}$, comprised of $\mathcal{E}_0$ and $\mathcal{E}_{\rm FID}$, is substantially different from $\mathcal{E}_0$. To model propagation of the mm waves in that case, we solved the coupled Maxwell-Bloch equations [27], which confirmed the value of n and demonstrated that $\mathcal{P}$ and $\mathcal{E}_{\rm eff}$ vary significantly along the Rydberg sample as well as with time. Optical thickness in systems with sufficiently long coherence times was related [9] to superradiance; we shall discuss cooperative effects in our Rydberg CPmmW experiment next.

In a polarized Rydberg gas the particles interact via long-range dipole–dipole interaction [28–30], which adds a random phase shift and can cause dephasing of the FID. Ensemble averaging over velocities and positions in a sample of strongly interacting particles gives [31] a rather simple expression

$$T_{\rm dd}^{-1} = \frac{\pi^2\mu^2 n}{\hbar} \qquad (1)$$

for the dipole–dipole dephasing rate. Using $n \approx 1\times10^6$ cm^{-3} we estimate the broadening, $\Delta\nu_{\rm dd} = \pi\mu^2 n/\hbar = 35$ kHz, which is not expected to make a noticeable contribution to the linewidth in the present experimental configuration.

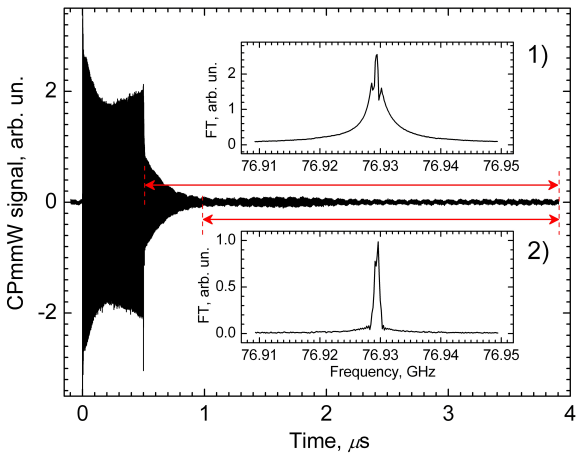

FIG. 4. Evidence of superradiant decay. The excitation pulse (0–0.5 μs) followed by FID (superradiance) (0.5–3.9 μs) is a continuation of the Fig. 3b, c series with $\mathcal{E}_0$=0.039 V/m ($\approx 1.4\times10^{-9}$ W), as determined by the tunable power attenuator. The line splitting in 1) is due to Zeeman effect. The observed ($1/e$) decay time of 190 ns is close to the predicted $T_{\rm sr} = 350$ ns. The inserts show Fourier transforms of different time intervals of the time-domain signal. 1) 0.5–3.9 μs: broader Lorentzian-type lineshape; 2) 1.0–3.9 μs: narrower Gaussian-type lineshape. This measurement is consistent with fast initial superradiant decay followed by slower, Doppler dephasing.

In extended ($L \gg \lambda$) samples, propagation of the FID would have a more prominent effect on the lineshape than the local dipole fields. The FID emitted in one part of the sample would interact with particles along the propagation path with the Rabi frequency $\Omega'_{\rm R} = \frac{\mu\mathcal{E}_{\rm FID}}{\hbar}$. The interaction of the particles with the common field and thus with each other is known [4, 6] to lead to accelerated coherent decay, or superradiance [4–11]. The characteristic rate $T_{\rm sr}^{-1} = \Omega'_{\rm R}$ of photon exchange between the particles can be found by approximating the mean strength of the FID field in our sample as $\bar{\mathcal{E}}_{\rm FID} \approx 4\pi^2\bar{\mathcal{P}}\frac{L}{2\lambda}$, $\bar{\mathcal{P}} \approx \frac{\mu n}{2}$, to be

$$T_{\rm sr}^{-1} \approx \frac{\pi^2\mu^2 n}{\hbar}\frac{L}{\lambda}, \qquad (2)$$

which is the expression for the superradiant decay time $T_{\rm sr}$ [6]. It can be noted that when the superradiance is not dephased by other mechanisms, its rate is $\sim\frac{L}{\lambda}$ times faster than the local dipole–dipole dephasing rate, and it is expected to determine the overall decay rate and the linewidth in this experiment. The observed decay time of 190 ns (Fig. 4) is in good agreement with $T_{\rm sr} = 350$ ns, and is consistent with FID evolving to superradiant decay. Studies with more spatially uniform samples of Ry-

dberg atoms and molecules are in progress. Although ion formation by the lasers could contribute to the decay time, it is not a major factor here. The broadening is decreasing with time and, in the case of ions, the nutations would decay much faster at early times than is observed. The stray-field broadening would result in a pronounced line asymmetry [20], which is not observed here.

Since superradiance is a coherent process, the best Signal × Resolution is expected to be reached when $T_{\rm sr} \sim T$:

$$q = \frac{\pi^2 \mu^2 n T}{\hbar} \frac{L}{\lambda} \sim 1, \qquad (3)$$

where T is the time constant of the prevailing dephasing or non-superradiant decay. The superradiant regime corresponds to higher values ($q \gg 1$) of this unitless quality parameter q [9]. Superradiant ringing [6, 10] and its dephasing, similar to what was observed here for transient nutations, are possible when $q \gg 1$. In our case $q = 3$, which shows that the present combination of parameters (n, μ, L, T) is close to optimal for high-resolution ($q \lesssim 1$) CPmmW spectroscopy.

Application of Rydberg CPmmW spectroscopy to molecules is the logical (and planned) continuation of the present work. The problem of fast (∼10 ns in NO [32] and ∼10 ps in HfF [33]) predissociation and autoionization of low-ℓ core-penetrating states can be remedied, for example, by Stark mixing the short-lived low-ℓ states, accessible via laser excitation, into long-lived, high-ℓ, core-nonpenetrating states. Alternatively, application of successive mm-wave pulses, which can be crafted with the AWG, can assist in climbing the ladder of n^*, ℓ Rydberg states until one with a lifetime $\gtrsim 1$ μs is reached and sufficiently long-lived FID can be recorded. Rydberg CPmmW experiments open possibilities for coherent manipulations of Rydberg states and rovibronic state-specific preparation of molecular ions via vibrational autoionization of core-nonpenetrating Rydberg states, which could be valuable for electron electric dipole moment experiments [33]. Investigation of the collective Lamb shift [34] in extended samples with $q \gg 1$ is another interesting direction for future CPmmW experiments.

Concluding, we have directly detected coherent mm-wave radiation from Rydberg–Rydberg transitions in a cavity-free experiment. Broadband mm-wave spectroscopy of Rydberg atoms was demonstrated, and coherent effects in an optically thick Rydberg gas were observed.

The authors are grateful to Prof. Brooks Pate and Justin Neill for assistance in the construction of the CPmmW spectrometer and to Prof. Daniel Kleppner for reading the manuscript and making valuable comments. We acknowledge the assistance from the iOpenShell Center. This work is supported by a grant from the National Science Foundation (CHE-0749821).

* Present address: Department of Physics, Stanford University, Stanford, CA 94305
† E-mail: rwfield@mit.edu

[1] T. F. Gallagher, *Rydberg Atoms* (Cambridge University Press, 1994).
[2] F. Merkt and A. Osterwalder, Int. Rev. Phys. Chem. **21**, 385 (2002).
[3] S. R. Lundeen, in *Advances in Atomic, Molecular and Optical Physics*, Vol. 52, edited by P. R. Berman and C. C. Lin (Elsevier, 2005).
[4] R. H. Dicke, Phys. Rev. **93**, 99 (1954).
[5] N. Skribanowitz, I. P. Herman, J. C. MacGillivray, and M. S. Feld, Phys. Rev. Lett. **30**, 309 (1973).
[6] J. C. MacGillivray and M. S. Feld, Phys. Rev. A **14**, 1169 (1976).
[7] M. Gross *et al.*, Phys. Rev. Lett. **43**, 343 (1979).
[8] L. Moi *et al.*, Opt. Commun. **33**, 47 (1980).
[9] R. Friedberg and S. R. Hartmann, Phys. Lett. A **37**, 285 (1971).
[10] M. Gross and S. Haroche, Phys. Rep. **93**, 301 (1982).
[11] R. L. Shoemaker, in *Laser and Coherence Spectroscopy*, edited by J. I. Steinfeld (Plenum Press, New York, 1978).
[12] P. J. Tanner, J. Han, E. S. Shuman, and T. F. Gallagher, Phys. Rev. Lett. **100**, 043002 (2008).
[13] M. D. Lukin *et al.*, Phys. Rev. Lett. **87**, 037901 (2001).
[14] G. G. Brown *et al.*, Rev. Sci. Instrum. **79**, 053103 (2008).
[15] B. C. Dian, G. G. Brown, K. O. Douglass, and B. H. Pate, Science **320**, 924 (2008).
[16] G. B. Park, A. H. Steeves, K. Kuyanov-Prozument, J. L. Neill, and R. W. Field, (2011), (accepted to J. Chem. Phys.).
[17] J. J. Kay *et al.*, Can. J. Chem. **82**, 791 (2004).
[18] J. J. Kay *et al.*, J. Chem. Phys. **128**, 194301 (2008).
[19] D. Dill and C. Jungen, J. Phys. Chem. **84**, 2116 (1980).
[20] A. Osterwalder and F. Merkt, Phys. Rev. Lett. **82**, 1831 (1999).
[21] T. R. Gentile, B. J. Hughey, D. Kleppner, and T. W. Ducas, Phys. Rev. A **42**, 440 (1990).
[22] H. C. Torrey, Phys. Rev. **76**, 1059 (1949).
[23] G. B. Hocker and C. L. Tang, Phys. Rev. Lett. **21**, 591 (1968).
[24] J. C. McGurk, R. T. Hofmann, and W. H. Flygare, J. Chem. Phys. **60**, 2922 (1974).
[25] M. L. Zimmerman, M. G. Littman, M. M. Kash, and D. Kleppner, Phys. Rev. A **20**, 2251 (1979).
[26] B. R. Mollow, Phys. Rev. **188**, 1969 (1969).
[27] A. Icsevgi and W. E. Lamb, Phys. Rev. **185**, 517 (1969).
[28] J. M. Raimond, G. Vitrant, and S. Haroche, J. Phys. B **14**, L655 (1981).
[29] T. F. Gallagher and P. Pillet, in *Advances in Atomic, Molecular and Optical Physics*, Vol. 56, edited by E. Arimondo, P. R. Berman, and C. C. Lin (Elsevier, 2008).
[30] K. Afrousheh *et al.*, Phys. Rev. Lett. **93**, 233001 (2004).
[31] V. M. Akulin and N. V. Karlov, *Intense Resonant Interactions in Quantum Electronics* (Springer-Verlag, Berlin, 1992) pp. 140–146.
[32] M. J. J. Vrakking, J. Chem. Phys. **105**, 7336 (1996).
[33] E. A. Cornell *et al.*, (OSU International Symposium on Molecular Spectroscopy, 2010, Abstract MA01).
[34] M. O. Scully and A. A. Svidzinsky, Science **328**, 1239 (2010).